Appl. Phys. B 90, 465–469 (2008)
DOI: 10.1007/s00340-007-2913-2

Applied Physics B
Lasers and Optics

C. BOUZIDI
A. MOADHEN✉
H. ELHOUICHET
M. OUESLATI

Er^{3+}-doped sol–gel SnO_2 for optical laser and amplifier applications

Unité de Spectroscopie Raman, Département de Physique, Faculté des Sciences de Tunis, 2092 El Manar Tunis, Tunisia

Received: 25 June 2007 / Revised version: 7 December 2007
Published online: 19 January 2008 •

ABSTRACT Erbium-doped tin dioxide (SnO_2:Er^{3+}) was obtained by the sol–gel method. Spectroscopic properties of the SnO_2:Er^{3+} are analyzed from the Judd–Ofelt (JO) theory. The JO model has been applied to absorption intensities of Er^{3+} ($4f^{11}$) transitions to establish the so-called Judd–Ofelt intensity parameters: Ω_2, Ω_4, and Ω_6. With the weak spectroscopic quality factors Ω_4/Ω_6, we expect a relatively prominent infrared laser emission. The intensity parameters are used to determine the spontaneous emission probabilities of some relevant transitions, the branching ratios, and the radiative lifetimes of several excited states of Er^{3+}. The emission cross section (1.31×10^{-20} cm^2) is evaluated at 1.54 μm and was found to be relatively high compared to that of erbium in other systems. Efficient green and red up-conversion luminescence were observed, at room temperature, using a 798-nm excitation wavelength. The green up-conversion emission is mainly due to the excited state absorption from $^4I_{11/2}$, which populates the $^4F_{3/2,5/2}$ states. The red up-conversion emission is due to the energy transfer process described by Er^{3+} ($^4I_{13/2}$) + Er^{3+}($^4I_{11/2}$) → Er^{3+}($^4F_{9/2}$) + Er^{3+} ($^4I_{15/2}$) and the cross-relaxation process. The efficient visible up-conversion and infrared luminescence indicate that Er^{3+}-doped sol–gel SnO_2 is a promising laser and amplifier material.

PACS 71.20.Eh; 74.25.Gz; 78.55.-m

1 Introduction

For about 40 years, much attention has been devoted to the research of the rare-earth (RE) ions like Er^{3+} for doping of materials [1–5] due to the 1.54-μm emission from the $^4I_{13/2} \rightarrow {}^4I_{15/2}$ transition of the Er^{3+} ions being eye-safe and located in the optical communication window. At present, the Er^{3+}-ion-doped materials have been used as a medium of the up-conversion laser, i.e. the erbium-doped fiber amplifier (EDFA) that is one of the key elements used in wavelength-division-multiplexing (WDM) network systems for optical communication, data storage, biomedical imaging, etc. [6–8].

Based on the Judd–Ofelt (JO) theory [9, 10], spectroscopic properties of Er^{3+} ions in many materials have been widely studied [1–5]. By changing the host material composition and Er^{3+}-doping concentration, the spectroscopic parameters of Er^{3+} ions, which are used to estimate the laser performances of the materials, can be modified. Among the parameters, the luminescence lifetime and the radiative quantum efficiency of the upper level in laser operation, such as the $^4I_{13/2}$ state of Er^{3+} ions for the 1.54-μm laser emission, are directly related to the effect of laser performance and treated as key parameters in the spectroscopic analysis. The spectroscopic analysis for many other Er^{3+}-doped materials like transparent conducting oxides (TCOs) still remains scanty and incomplete.

The use of the sol–gel technique in preparation of TCOs and glasses of high purity and homogeneity for various electro-optic and photonic applications is relatively new. Rare-earth ions incorporated into glasses, thin films, and nanoparticles via the sol–gel process enable the design of host materials. Currently, there is a growing interest in the study of new host materials prepared by the sol–gel technique. The sol–gel route presents some advantages such as the possibility of deposition on complex shapes, an easy control of the doping level, rather inexpensive starting materials, and simple equipment. Although the sol–gel materials doped with REs are well studied, just a few works have investigated the Judd–Ofelt theory, which is reserved essentially for RE-doped glasses.

In the present study, we show that the JO theory can be applied to sol–gel materials doped with REs. We have performed an in-depth JO analysis of erbium-doped tin dioxide obtained by the sol–gel method. The JO spectroscopic analyses are performed using the high-resolution room-temperature absorption spectrum. The infrared and up-conversion emission properties of Er^{3+} are studied and discussed.

2 Experimental procedure

2.1 *Sample preparation*

The solutions were prepared as follows: 8.37 g of $SnCI_2$:$2H_2O$ was dissolved in 100 ml of absolute ethanol. This mixture was stirred and heated at 83 °C for 2 h in a closed vessel. Then the vessel was opened, and the solution was again stirred and heated until the solvent was completely evaporated. The final result was a powder, to which 50 ml of absolute ethanol was added. The final SnO_2 solution was then stirred and heated for 2 h at 50 °C. An appropriate quantity of

✉ Fax: +216-71-885-073, E-mail: adel.moadhen@fst.rnu.tn

erbium trichloride ($ErCl_3$) was dissolved in the prepared SnO_2 solution. The doped mixture was finally stirred and heated at 50 °C for 2 h.

SnO_2:Er^{3+} (3 at. %) films deposited on quartz were prepared using the dip-coating procedure. The deposited layer was then dried in air at 150 °C for 30 min after each dipping. Then, the SnO_2:Er^{3+} films were annealed by classic thermal annealing at 450 °C for 30 min to assure the crystallization of SnO_2 and then to 1050 °C for 5 min in order to activate the Er^{3+} ions in the matrix. To obtain a satisfactory film thickness for practical application, the above cycle (dipping–drying–heating) was repeated several times (up to 20 times). The thickness of the SnO_2:Er^{3+} (3 at. %) film is about 1 mm.

2.2 *Optical measurements*

Infrared photoluminescence (PL) measurements are performed by using the excitation wavelength 488 nm from an argon laser and a monochromator with an InGaAs photodiode. From a titanium–sapphire laser, pumped by the argon laser, the 798-nm line is selected as excitation wavelength for the study of the up-conversion emission.

The absorption spectrum of the sample was measured by a Bruker IFS 66 v/S spectrometer. All the optical measurements were performed at room temperature.

3 Data analysis

3.1 *Absorption measurement*

The absorption spectrum of SnO_2:Er^{3+} (3 at. %) (Fig. 1) consists of 10 absorption bands peaked at 1536.6, 981.4, 811.5, 674.5, 530.8, 518.3, 491.6, 450.8, 443.6, and 417.8 nm, corresponding to the absorptions from the ground state $^4I_{15/2}$ to the excited states $^4I_{13/2}$, $^4I_{11/2}$, $^4I_{9/2}$, $^4F_{9/2}$, $^4S_{3/2}$, $^2H_{11/2}$, $^4F_{7/2}$, $^4F_{5/2}$, $^4F_{3/2}$, and $^2G_{9/2}$, respectively.

3.2 *Judd–Ofelt parameters*

The data from the absorption spectrum can be used to predict the important spectroscopic parameters for the corresponding Er^{3+} ($4f^{11}$) transitions in doped SnO_2 from the sol–gel method such as the radiative transition probabilities, the branching ratios, and the radiative lifetime of different transitions, in particular from $^4I_{13/2}$ to the ground state (1.53 μm).

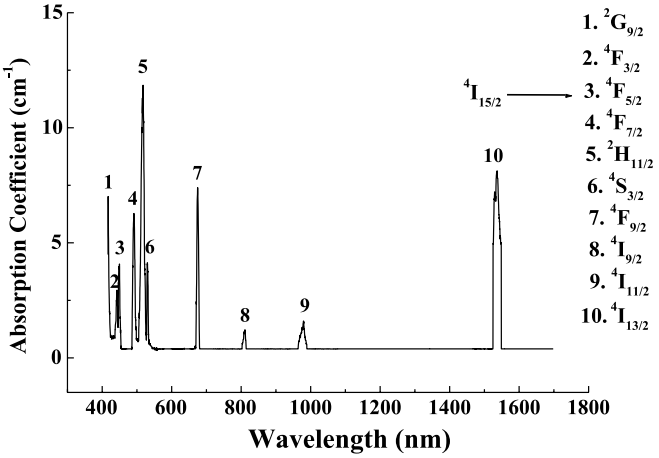

FIGURE 1 Optical absorption spectrum of SnO_2:Er^{3+} (3 at. %)

The measured absorption line strengths (S_{meas}) for the induced electric dipole transition of each band were determined using the following expression:

$$S_{meas}(J \to J') = \frac{3ch(2J+1)}{8\pi^3\lambda e^2 N_0}\left[\frac{9n}{(n^2+2)^2}\right]\Gamma\,, \qquad (1)$$

where J and J' represent the total angular momentum quantum numbers of the initial and final levels, respectively, n is the refractive index, N_0 is the Er^{3+}-ion concentration per unit volume (the corresponding Er^{3+} concentration was determined to be 8.27×10^{20} cm^{-3} in SnO_2), λ is the mean wavelength of the specific absorption band that corresponds to the $J \to J'$ transition, $\Gamma = \int \alpha(\lambda)\,\mathrm{d}\lambda$ is the integrated absorption coefficient as a function of λ, c is the velocity of light in vacuum, and h is the Planck constant. The refractive index n of SnO_2 from the sol–gel method is about 1.76 and is supposed to be practically unchanged with λ [11]. The factor $[9/(n^2+2)^2]$ in (1) represents the local field correction for the ion in the dielectric host medium and e is the charge of the electron.

The measured line strengths are then used to obtain the JO parameters Ω_2, Ω_4, and Ω_6 by solving the set of equations for the corresponding transitions between J and J' manifolds in the following form:

$$S_{calc}(J \to J') = \sum_{t=2,4,6} \Omega_t |\langle (S, L)J||U^{(t)}||(S', L')J'\rangle|^2\,, \qquad (2)$$

where Ω_2, Ω_4, and Ω_6 are the Judd–Ofelt intensity parameters and $\langle||U^{(t)}||\rangle$ are the doubly reduced matrix elements of rank t ($t = 2, 4, 6$) between states characterized by the quantum numbers (S, L, J) and (S', L', J'). The matrix elements are independent of the host material and can be easily calculated from the tables of Nielson and Koster [12]. The JO parameters, however, exhibit the influence of the host on the transition probabilities since they contain the crystal-field parameters, interconfigurational radial integrals, and the interaction between the central ion and the intermediate environment. We have used the values of the reduced matrix elements for the chosen Er^{3+} bands calculated by Carnall et al. [13]. When three absorption manifolds overlapped, the squared matrix element was taken to be the sum of the corresponding squared matrix elements.

The values of average wavelength, integrated absorption coefficients, and measured (S_{meas}) and calculated (S_{calc}) absorption line strengths for absorption transitions of Er^{3+}-doped SnO_2 from the sol–gel method are tabulated in Table 1.

A measure of the accuracy of the fit is given by the rms deviation:

$$\Delta S_{rms} = \left[(q-p)^{-1}\sum(\Delta S)^2\right]^{\frac{1}{2}}\,,$$

where $\Delta S = S_{calc} - S_{meas}$ is the deviation, q is the number of analyzed spectral bands, and p is the number of the parameters sought, which in this case is three. The calculated value of ΔS_{rms} is 0.376×10^{-20} cm^2.

A least-squares fitting of S_{calc} to S_{meas} provides the three JO parameters for Er^{3+} in sol–gel SnO_2. The JO intensity parameters give an insight into the local structure and bonding in the vicinity of the rare-earth ions. The environment-sensitive parameter (Ω_2) indicates an amount of covalent bonding and the vibronic-dependent parameter (Ω_6) is related to the rigidity of the material. The JO intensity parameters obtained are $\Omega_2 = 3.72 \times 10^{-20}\,cm^2$, $\Omega_4 = 0.90 \times 10^{-20}\,cm^2$, and $\Omega_6 = 1.02 \times 10^{-20}\,cm^2$. The large values of Ω_2 and Ω_6, compared to Er-doped sol–gel SiO_2 (Table 2 [14]), indicate, respectively, high covalency and high rigidity of the metal–ligand bond.

According to the Jacobs and Weber theory [15], the erbium emission intensity could be characterized uniquely by the Ω_4 and Ω_6 parameters. Thus, we use the so-called spectroscopic quality factor, equal to the ratio Ω_4/Ω_6. The smaller this parameter value, the more intense the laser transition $^4I_{13/2} \rightarrow {}^4I_{15/2}$ is. For Er^{3+} in SnO_2, this parameter is estimated to be 0.88, which indicates that the last transition is more efficient than in other host materials (Table 2).

The emission peak position is related to the covalence degree of the Er^{3+}–ligand bonds in the matrix. The more covalent these bonds, the weaker the electron–electron interaction in the $4f$ shell and the lower the transition energy are. Based on the above-mentioned arguments, the obtained value of the $^4I_{13/2} \rightarrow {}^4I_{15/2}$ emission peak wavelength (1.54 μm) suggests that, in this matrix, the Er^{3+} ion interacts strongly with its ligands.

The JO parameters can now be applied to (2) to calculate the emission line strengths corresponding to the transitions from the upper manifold states, $^4I_{13/2}$, $^4I_{11/2}$, $^4F_{9/2}$, $^4S_{3/2}$, and $^2H_{11/2}$, to their corresponding lower-lying manifold states. Using these line strengths, the radiative lifetime (τ_r) for transitions between an excited state and the total spontaneous transition probability, $A_{tot}(J \rightarrow J')$, can be calculated using the following expression:

$$A_{tot}(J \rightarrow J') = A_{ed} + A_{md} = \frac{64\pi^4 e^2}{3h(2J+1)\lambda^3}\left[\frac{n(n^2+2)^2}{9} S_{ed} + n^3 S_{md}\right], \quad (3)$$

where A_{ed} and A_{md} are the electric-dipole and magnetic-dipole spontaneous emission probabilities, respectively. The electric-dipole line strength S_{ed} is calculated using (2) and presents a host dependence through the Ω_t parameters. The magnetic-dipole line strength S_{md} can be calculated with the expression

$$S_{md} = \frac{h^2}{16\pi^2 m^2 c^2} |\langle (S, L)J || L + 2S || (S', L')J' \rangle|^2 .$$

In this work, the values of A_{md} were calculated using the values for LaF_3 (A'_{md}) and corrected for the refractive-index difference [18, 19]. The relationship is

$$A_{md} = \left(\frac{n}{n'}\right)^3 A'_{md} ,$$

where n and n' are the refractive indices of erbium-doped SnO_2 from the sol–gel method and LaF_3, respectively.

The radiative lifetime τ_r of an emitting state is related to the total spontaneous transition probability for all transitions from this state by

$$\tau_r = \frac{1}{\sum_{J'} A_{tot}(J \rightarrow J')} .$$

TABLE 1 Values of the average wavelengths, integrated absorption coefficients, and experimental and calculated line strengths of Er^{3+}-doped SnO_2 at 300 K

Transition from $^4I_{15/2}$ to	λ_{abs} (nm)	Γ (nm cm^{-1})	S_{meas} (10^{-20} cm^2)	S_{calc} (10^{-20} cm^2)
$^4I_{13/2}$	1536.6	159.434	1.278	1.637
$^4I_{11/2}$	981.4	28.248	0.354	0.508
$^4I_{9/2}$	811.5	11.792	0.179	0.166
$^4F_{9/2}$	674.5	47.661	0.870	0.952
$^4S_{3/2}$	530.8	27.248	0.632	0.225
$^2H_{11/2}$	518.3	131.812	3.132	3.115
$^4F_{7/2}$	491.6	50.040	1.253	0.770
$^4F_{5/2}$	450.8	24.182	0.660	0.227
$^4F_{3/2}$	443.6	17.484	0.485	0.130
$^2G_{9/2}$	417.8	20.040	0.590	0.247

TABLE 2 Judd–Ofelt parameters of the erbium in different host materials

Host materials	Ω_2 (10^{-20} cm^2)	Ω_4 (10^{-20} cm^2)	Ω_6 (10^{-20} cm^2)	Ω_4/Ω_6
Er^{3+}: monolithic sol–gel glasses [14]	1.9	0.7	0.9	0.77
Er^{3+}: gallium tellurite glasses [16]	6.64	1.64	1.47	1.11
Er^{3+}: tellurite glasses [17]	5.98	1.32	1.47	0.89
Er^{3+}:Na_2O–Nb_2O_5–TeO_2 glasses [18]	6.86	1.53	1.12	1.36
Present work SnO_2:Er^{3+}	3.72	0.90	1.02	0.88

Transition	λ (nm)	A_{ed} (s^{-1})	A_{md} (s^{-1})	A (s^{-1})	β	τ_r (ms)
$^4I_{13/2} \rightarrow {}^4I_{15/2}$	1536.6	118.46	52.41	170.87	1.000	5.85
$^4I_{11/2} \rightarrow {}^4I_{15/2}$	981.4	164.62		164.62	0.833	5.06
$\rightarrow {}^4I_{13/2}$	2716.2	21.15	11.69	32.84	0.166	
$^4F_{9/2} \rightarrow {}^4I_{15/2}$	674.5	1140.50		1140.50	0.901	0.79
$\rightarrow {}^4I_{13/2}$	1202.2	52.51		52.51	0.041	
$\rightarrow {}^4I_{11/2}$	2156.9	57.90	8.23	66.13	0.052	
$\rightarrow {}^4I_{9/2}$	3995.3	2.16	3.88	6.04	0.004	
$^4S_{3/2} \rightarrow {}^4I_{15/2}$	530.8	1384.50		1384.50	0.652	0.47
$\rightarrow {}^4I_{13/2}$	810.9	608.02		608.02	0.286	
$\rightarrow {}^4I_{11/2}$	1156.0	47.05		47.05	0.022	
$\rightarrow {}^4I_{9/2}$	1534.5	83.91		83.91	0.039	
$\rightarrow {}^4F_{9/2}$	2491.4	0.28		0.28	0.001	
$^2H_{11/2} \rightarrow {}^4I_{15/2}$	518.3	6853.40		6853.40	0.966	0.14
$\rightarrow {}^4I_{13/2}$	782.1	124.34		124.34	0.017	
$\rightarrow {}^4I_{9/2}$	1434.5	116.56		116.56	0.016	

TABLE 3 Calculated radiative parameters of Er^{3+} ions in SnO_2 sol–gel matrix

The fluorescence branching ratios, $\beta(J \rightarrow J')$, can be determined from the radiative decay rates by

$$\beta(J \rightarrow J') = \frac{A_{tot}(J \rightarrow J')}{\sum A_{tot}(J \rightarrow J')} = A_{tot}(J \rightarrow J')\tau_r ,$$

where the sum runs over all final states J'. The luminescence branching ratio is a critical parameter to the laser designer, because it characterizes the possibility of attaining stimulated emission from any specific transition.

Table 3 shows the values of the theoretically computed electric-dipole spontaneous emission probability (A_{ed}), magnetic–dipole spontaneous emission probability (A_{md}), total spontaneous transition probability (A_{tot}), fluorescence branching ratio (β), and radiative lifetime (τ_r) of various excited states of Er^{3+}-doped SnO_2.

3.3 *Infrared emission spectrum and cross section*

Figure 2 shows the PL spectrum in the infrared (IR) region of SnO_2:Er^{3+} films. The IR PL peaks localized at 814, 983, and 1541 nm correspond to the $^4I_{9/2} \rightarrow {}^4I_{15/2}$, $^4I_{11/2} \rightarrow {}^4I_{15/2}$, and $^4I_{13/2} \rightarrow {}^4I_{15/2}$ transitions, respectively.

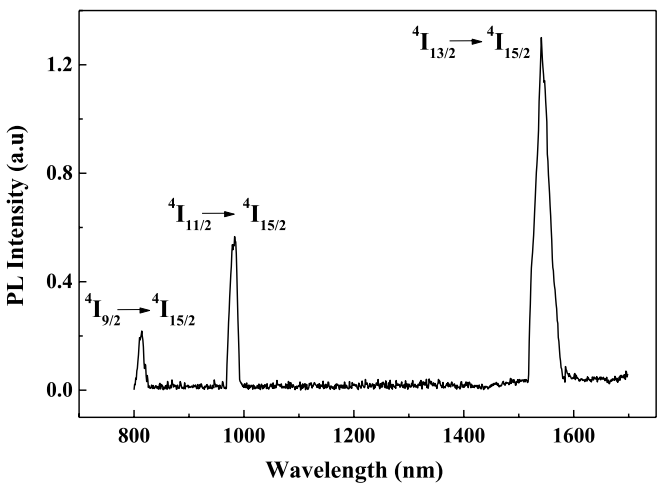

FIGURE 2 Infrared photoluminescence spectrum of Er^{3+}-doped sol–gel SnO_2

The PL peaks are not well resolved, indicating that Er^{3+} ions occupy multi-sites in the SnO_2 matrix. We have shown in previous works [20, 21] from the analysis of the PL decay of rare-earth ions in SnO_2 and porous materials that these ions occupy multi-sites. In fact, the experimental PL decay curves are well described by a stretched exponential function, indicating a distribution of the lifetime.

The emission cross section of the $^4I_{13/2} \rightarrow {}^4I_{15/2}$ transition has been obtained from the line shape of the emission spectrum. Its expression is [22]

$$\sigma_e = \frac{\lambda e^4 A_{tot}}{8\pi c n^2 \Delta\lambda_{eff}} ,$$

where λ_e is the peak emission, n is the refractive index, A_{tot} is the total spontaneous transition probability, and $\Delta\lambda_{eff}$ is the effective line width given by

$$\Delta\lambda_{eff} = \frac{\int I(\lambda)\,d\lambda}{I_{max}} ,$$

in which $I(\lambda)$ is the emission intensity at the wavelength λ and I_{max} is the emission intensity at the peak emission wavelength.

The maximum emission cross section is estimated to be $1.31 \times 10^{-20}\,cm^2$ at 1541 nm. This value is larger than the values obtained for erbium in Na_2O–Nb_2O_5–TeO_2 glasses [18] ($1.02 \times 10^{-20}\,cm^2$) and in tellurite glass [17] ($0.84 \times 10^{-20}\,cm^2$). Such a result shows the performance of sol–gel materials in the optical properties of RE ions.

3.4 *Up-conversion luminescence and mechanisms analysis*

Erbium in SnO_2 shows an up-conversion emission, at room temperature, when pumped with a 798-nm line (Fig. 3). The PL spectrum exhibits three distinct emission bands. The green luminescence corresponding to the ($^2H_{11/2}$, $^4S_{3/2}$) $\rightarrow {}^4I_{15/2}$ transitions of Er^{3+} at 518 nm and 545 nm can readily be seen by the naked eye for pump powers lower than 90 mW. This observation indicates a considerably efficient up-conversion process in such a host sol–gel material. Figure 3 also shows a red emission band centered at 648 nm attributed to the $^4F_{9/2} \rightarrow {}^4I_{15/2}$ transition.

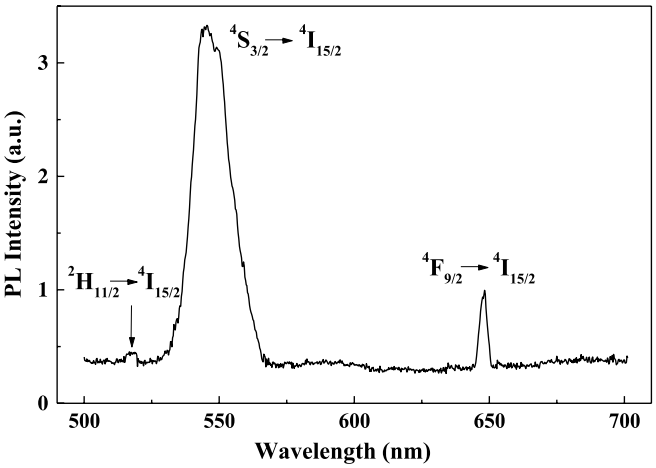

FIGURE 3 Visible up-conversion spectrum of SnO_2:Er^{3+} (3 at. %) excited from the 798-nm wavelength

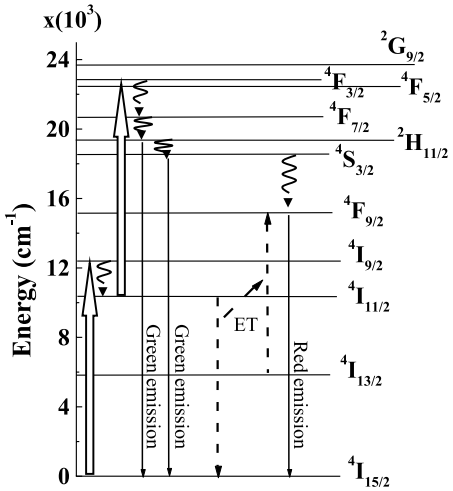

FIGURE 4 Energy level diagram of SnO_2:Er^{3+}. Possible visible up-conversion emission mechanisms under 798-nm excitation are indicated

The up-conversion emission for the three emission bands could be related to a two-photon absorption process. This result has been reported elsewhere for other host materials [16–18, 23, 24]. The possible up-conversion mechanisms for the three emission bands are discussed as follows. Absorption of laser photons (798 nm) raises Er^{3+} ions from the ground state to the $^4I_{9/2}$ state, which undergoes multiphonon relaxation to the $^4I_{11/2}$ state. The ions in the $^4I_{11/2}$ state sequentially absorb laser photons (798 nm) and are raised to $^4F_{3/2,5/2}$ states. The ions in the $^4F_{3/2,5/2}$ states undergo multiphonon relaxation through $^4F_{7/2}$ to $^2H_{11/2}$ and $^4S_{3/2}$ states. Because the energy gap below the $^4S_{3/2}$ state is larger, the multiphonon relaxation rate from the $^4S_{3/2}$ state becomes smaller. Therefore, the strong green luminescence was emitted through $^4S_{3/2} + {}^2H_{11/2} \rightarrow {}^4I_{15/2}$ transitions. For the red up-conversion, the population of the $^4F_{9/2}$ level is the combined result of energy transfer (ET) from the $^4I_{13/2}$ level and a contribution from higher-energy levels by non-radiative relaxation. The energy transfer process can be described as Er^{3+} ($^4I_{13/2}$) + Er^{3+} ($^4I_{11/2}$) → Er^{3+}($^4F_{9/2}$) + Er^{3+} ($^4I_{15/2}$), and it is a dominant contribution to red up-conversion because the cross relaxation should be efficient due to the high population of the $^4I_{13/2}$ level.

The energy levels illustrating the up-conversion process under 798-nm excitation are shown in Fig. 4.

4 Conclusion

Er^{3+}-doped tin dioxide has been obtained by the sol–gel method. The JO intensity parameters, the oscillator strengths, the spontaneous transition probabilities, the branching ratios, and the radiative lifetimes were successfully calculated based on the experimental absorption spectrum and the JO theory. A weak spectroscopic quality factor Ω_4/Ω_6 is obtained. It indicates that the infrared laser emission is relatively intense. The calculated spontaneous transition probability for 1536-nm luminescence is 170.9 s^{-1} and the emission cross section is 1.31×10^{-20} cm^2. Efficient green and red up-conversion luminescence, and intense broad 1.54-μm infrared PL, were observed. The up-conversion mechanisms mainly involve excited state absorption and energy transfer. A schematic diagram of the up-conversion process is proposed.

The results indicate that SnO_2:Er^{3+} obtained by the sol–gel method is a promising host in the development of rare-earth-doped transparent conducting oxides for laser and amplifier applications.

ACKNOWLEDGEMENTS The authors would like to thank Mr. R. Chtourou from the INRST for the PL measurements in the infrared range.

REFERENCES

1 Y.D. Huang, M. Mortier, F. Auzel, Opt. Mater. **17**, 501 (2001)
2 T.Y. Ivanova, A.A. Man'shina, A.V. Kurochkin, Y.S. Tver'yanovich, V.B. Smirnov, J. Non-Cryst. Solids **298**, 7 (2002)
3 J.H. Yang, S.X. Dai, Y.F. Zhou, L. Wen, L.L. Hu, Z.H. Jiang, J. Appl. Phys. **93**, 977 (2003)
4 H. Lin, K. Liu, E.Y.B. Pun, T.C. Ma, X. Peng, Q.D. An, J.Y. Yu, S.B. Jiang, Chem. Phys. Lett. **398**, 146 (2004)
5 J. Yang, S. Dai, N. Dai, L. Wen, L. Hu, Z. Jiang, J. Luminesc. **106**, 9 (2004)
6 N. Rakov, F.E. Romas, G. Hirata, M. Xiao, Appl. Phys. Lett. **83**, 272 (2003),
7 N. Chiodini, A. Palearia, G. Brambilla, E.R. Taylor, Appl. Phys. Lett. **80**, 4449 (2002)
8 Y. Chen, Y. Huang, Z. Luo, Chem. Phys. Lett. **382**, 481 (2003)
9 B.R. Judd, Phys. Rev. **127**, 750 (1962)
10 G.S. Ofelt, J. Chem. Phys. **37**, 511 (1962)
11 J.P. Chatelon, C. Terrier, E. Bernstein, R. Berjoan, J.A. Roger, Thin Solid Films **247**, 162 (1994)
12 C.W. Nielson, G.F. Koster, *Spectroscopic Coefficients for pn, dn and fn Configurations* (MIT Press, Cambridge, MA, 1964), pp. 53–63
13 W.T. Carnall, P.R. Fields, R. Rajnak, J. Chem. Phys. **49**, 4424 (1968)
14 K. Driesen, C. Görller-Walrand, K. Binnemans, Mater. Sci. Eng. C **18**, 255 (2001)
15 R.R. Jacobs, M.J. Weber, IEEE J. Quantum Electron. **QE-12**, 102 (1976)
16 H. Lin, K. Liu, E.Y.B. Pun, T.C. Ma, X. Peng, Q.D. An, J.Y. Yu, S.B. Jiang, Chem. Phys. Lett. **398**, 146 (2004)
17 G.A. Kumar, E. De la Rosa, H. Desirena, Opt. Commun. **260**, 601 (2006)
18 H. Lin, S. Jiang, J. Wu, F. Song, N. Peyghambarian, E. Pun, J. Phys. D Appl. Phys. **36**, 812 (2003)
19 M.J. Weber, Phys. Rev. **157**, 262 (1967)
20 H. Elhouichet, S. Daboussi, H. Ajlani, A. Najar, A. Moadhen, M. Oueslati, I.M. Tiginyanu, S. Langa, H. Föll, J. Luminesc. **113**, 329 (2005)
21 S. Dabboussi, H. Elhouichet, H. Ajlani, A. Moadhen, M. Oueslati, J.A. Roger, J. Luminesc. **121**, 507 (2006)
22 A.A. Kaminskii, *Laser Crystals, Their Physics and Properties* (Springer, Berlin, 1981)
23 N. Jaba, A. Kanoun, H. Mejri, A. Selmi, S. Alaya, H. Maaref, J. Phys.: Condens. Matter **12**, 4523 (2000)
24 A.M. Tkachuk, S.E. Ivanovab, M.-F. Joubertc, Y. Guyotc, L.I. Isaenkod, V.P. Gapontseve, J. Luminesc. **125**, 271 (2007)